

## INFLUENCES OF THE DIAMETER AND POSITION OF THE INNER HOLE ON THE STRENGTH AND FAILURE OF DISC SPECIMENS OF SANDSTONE DETERMINED USING THE BRAZILIAN SPLIT TEST

TANTAN ZHU

*State Key Laboratory of Coal Mine Disaster Dynamics and Control, Chongqing University, Chongqing, China*

DA HUANG

*School of Civil and Transportation Engineering, Hebei University of Technology, Tianjin, China*

*e-mail: dahuang@hebut.edu.cn*

The Brazilian split test on a centrally holed disc (referred to as a ring-disc specimen) is an important indirect method for determining the tensile strength of rock. This paper studies the effect of the diameter  $d$  of the center hole and its position, defined by the eccentricity  $b$  and the inclination angle of the eccentric hole, on the peak load, failure pattern and horizontal stress of the disc specimen via laboratory experiments and numerical modeling using the finite element method (FEM). Static Brazilian split tests are conducted on an intact disc and three types of holed discs: C-specimens containing a central hole with different diameters, EH-specimens with a horizontally eccentric hole and ER-specimens with a rotationally eccentric hole.

*Keywords:* Brazilian test, rock, eccentric hole, strength, failure pattern

### 1. Introduction

Crack initiation, propagation and coalescence in rocks is often caused by tensile stress (Song *et al.*, 2001; Shang *et al.*, 2008; Zhang *et al.*, 2014; Huang and Zhu, 2018). Thus, it is very important to determine the tensile strength of rocks. The Brazilian test is widely adopted as an indirect method that benefits from the compressive strength of rocks being much higher than their tensile strength. This test method has been widely used for more than 50 years (Mellor and Hawkes, 1971) and was recommended by the International Society of Rock Mechanics as one method to measure the tensile strength of rocks (ISRM, 1978) due to its simplicity of operation. Using the Brazilian split test method, the indirect tensile strength  $\sigma_t$  is given by the following analytic elastic solution (ISRM, 1978)

$$\sigma_t = \frac{2P_t}{\pi Dt} \quad (1.1)$$

where  $P_t$  is the peak vertical load and  $D$  and  $t$  are the diameter and the thickness of the disc, respectively.

The conventional Brazilian split test methods include flat loading platens, flat platens with cushion, flat loading platens with small diameter rods as well as curved loading jaws and others (Perras and Diederichs, 2014). Because the vertical load is applied in a narrow range of the disc using the above methods, crack initiation may occur at the position of the loading points, which may produce inaccurate results (Fairhurst, 1964; Mellor and Hawkes, 1971). To determine the tensile strength of brittle materials more precisely, discs with different shapes (Fowell, 1995; Lambert and Ross, 2000; Tong *et al.*, 2007; Dai *et al.*, 2010; Keles and Tutluoglu, 2011; Cai, 2013; Surendra, 2013; Hua *et al.*, 2015; Riazi *et al.*, 2015; Lin *et al.*, 2015, 2016) have been

proposed, including ring specimens that are placed under a pair of radial loads (Hobbs, 1964; Hudson, 1969). Significant stress and steep stress gradients appear in the specimens, which causes initiation and propagation of the resulting cracks (Wang *et al.*, 2014). Fischer *et al.* (1995) and Hossain *et al.* (2006) studied the features of both stress development and failure of discs with a central hole. Steen *et al.* (2005) investigated how the fracture patterns of discs are controlled by the size of the hole based on their horizontal diameters. A calculation of the tensile strength for discs with a hole located in their vertical or horizontal diameters was given by Hobbs (1965).

In this study, laboratory Brazilian split tests and numerical modeling using the finite element method (FEM) are conducted on three types of holed discs: discs with a central hole (C-specimen), discs containing a horizontally eccentric hole (EH-specimen) and discs with a rotationally eccentric hole (ER-specimen), which have rarely been studied in previous research. Based on the laboratory tests, the peak load and failure pattern of the discs are investigated. Moreover, the horizontal stress field in addition to the position and value of the maximum horizontal tensile stress are analyzed using the FEM. The simulated results further demonstrate the influence of the diameters and positions of the holes on the peak load and failure pattern of holed Brazilian disc specimens.

## 2. Test program

### 2.1. Specimen preparation

The tested sandstone specimens are light gray in color with some dark spots and lack visible cracks, holes and other defects. The average bulk density is  $2.36 \text{ g/cm}^3$ . The dimensions of the disc specimens obtained from a sandstone block are 30 mm in thickness  $T$  and 50 mm in diameter  $D$  after coring and grinding. In addition, an inner round hole with a smooth wall was drilled in the disc using high-strength ceramic bits. Three types of holed specimens – C-specimens, EH-specimens and ER-specimens – were manufactured, as illustrated in Fig. 1. In the figure,  $d$  is the diameter of the hole,  $b$  is the eccentricity (the distance between the two centers of the hole and disc), and  $\alpha$  is the angle between the horizontal line and the line segment connecting the centers of the disc and the hole. To recognize the two centers, two referenced lines are marked on the disc specimens. As shown in Fig. 1, VL is the vertical diameter line and the loading direction, and IL is a horizontal radial line for the C-specimens and an inclined radial line passing through the centers of the hole and the disc for the ER-specimens.

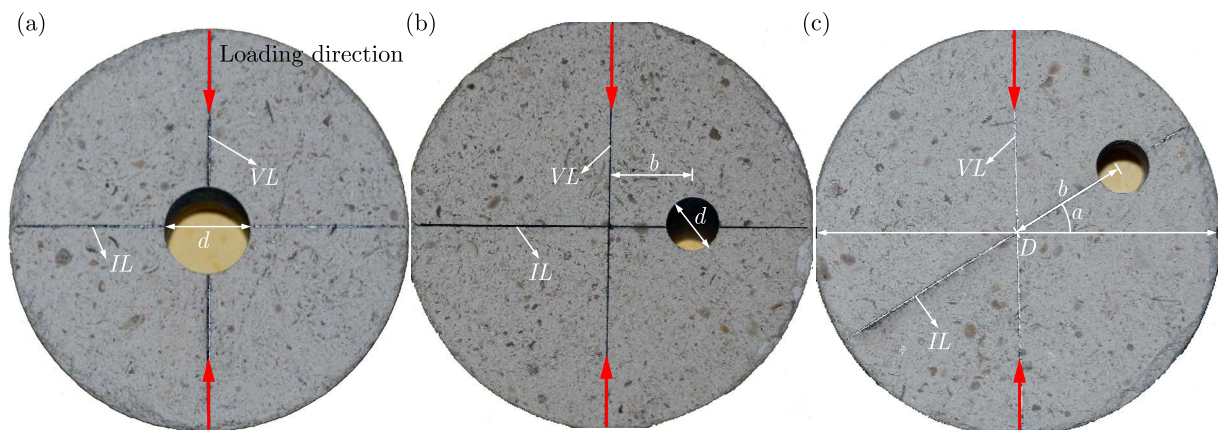


Fig. 1. Disc specimens containing a round hole: (a) C-specimen ( $\alpha = 0^\circ$ ,  $b = 0$  and  $d$  is variable); (b) EH-specimen ( $\alpha = 0^\circ$ ,  $d = 6 \text{ mm}$  and  $b$  is variable); (c) ER-specimen ( $b = 15 \text{ mm}$ ,  $d = 6 \text{ mm}$  and  $\alpha$  is variable)

## 2.2. Experimental scheme

Radial loading tests were conducted to investigate the strength and failure pattern of the discs with a hole of different diameters, eccentricities and inclination angles. The tests were performed using a DNS100 servo-controlled machine with the maximum loading capacity of 100 kN. The displacement-control mode with a constant loading rate of  $3.33 \times 10^{-4}$  mm/s was adopted. During the tests, a vertical load and a vertical displacement were recorded automatically by the test system. The geometry and location of the hole in the disc specimens are listed in Table 1, where two repeated tests for each specimen were conducted. As indicated in the table, the hole diameter  $d$  of the C-specimen (numbered Z1-1 to Z5-2) ranged from 4 mm to 12 mm with an interval of 2 mm; the eccentricity  $b$  ranged from 0 mm to 20 mm with an interval of 5 mm in the EH-specimens (numbered P1-1 to P4-2); and the ER-specimen (numbered Q1-1 to Q6-2) had an inclination angle  $\alpha$  of  $0^\circ$  to  $90^\circ$  with a  $15^\circ$  interval. The three intact specimens (referred to as without a hole) were numbered W1 to W3, separately. Based on the study by Mellor and Hawkes (1971), the calculated strength from the tests on the ring specimens was much higher than that by a direct tensile test when the hole diameter was very small. Thus, the same hole diameter of 6 mm for the EH-specimens and ER-specimens was considered moderate. The eccentricity was fixed at 15 mm in the ER-specimens.

**Table 1.** Geometry and location of the hole in the disc specimens

Specimen*	$d$ [mm]	$b$ [mm]	$\alpha$ [ $^\circ$ ]	Specimen*	$d$ [mm]	$b$ [mm]	$\alpha$ [ $^\circ$ ]	Specimen*	$d$ [mm]	$b$ [mm]	$\alpha$ [ $^\circ$ ]
Z1-1	4	0	–	P1-2	6	5	0	Q3-1	6	15	45
Z1-2	4	0	–	P2-1	6	10	0	Q3-2	6	15	45
Z2-1	6	0	–	P2-2	6	10	0	Q4-1	6	15	60
Z2-2	6	0	–	P3-1	6	15	0	Q4-2	6	15	60
Z3-1	8	0	–	P3-2	6	15	0	Q5-1	6	15	75
Z3-2	8	0	–	P4-1	6	20	0	Q5-2	6	15	75
Z4-1	10	0	–	P4-2	6	20	0	Q6-1	6	15	90
Z4-2	10	0	–	Q1-1	6	15	15	Q6-2	6	15	90
Z5-1	12	0	–	Q1-2	6	15	15	W1	Intact specimens		
Z5-2	12	0	–	Q2-1	6	15	30	W2			
P1-1	6	5	0	Q2-2	6	15	30	W3			

\* Z represents the specimen with a central hole;

P represents the specimen with a hole of varying eccentricities;

Q represents the specimen with a hole of varying inclination angle;

W represents intact specimens

## 3. Experimental results

### 3.1. Deformation and failure of the intact sample

Figure 2 gives the vertical load-displacement curves of the three intact specimens. Overall, the three load-displacement curves of the intact discs are similar in strength and deformation. The shape of the curves is slightly concave-up at the beginning stage due to gradual densification of the sample with micro defects. With an increase in the vertical load, the load-displacement curves gradually develop into the linear elasticity segments. The curves are characterized by a sudden force drop to zero, suggesting brittle failure immediately after the peak load.

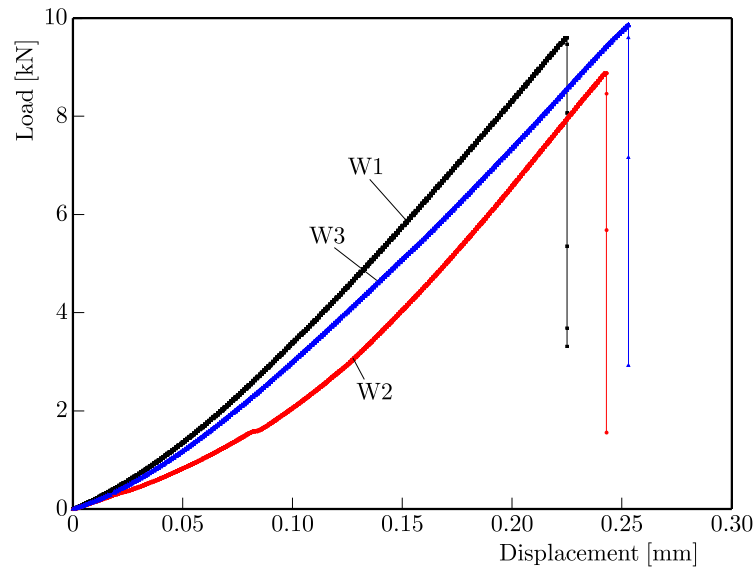


Fig. 2. Load-displacement curves of intact disc specimens

The peak loads of the three intact specimens are 9.60 kN, 8.88 kN and 9.87 kN. The corresponding tensile strengths calculated by Eq. (1.1) are 4.89 MPa, 4.52 MPa and 5.02 MPa, respectively. The dispersion coefficient (ratio of standard deviation to the mean) of the tensile strengths is only 4.4%, implying that the tested sandstone samples exhibited good homogeneity. The fractures of the intact specimens occurred only in the vertical direction through the approximate centers of the discs, as shown in Fig. 3. Additionally, distinctly opening fractures at the top or bottom of the specimens such as in W2 and W3 are observed. Hence, the center initiation, which is the basic hypothesis in the Brazilian split test, may be doubtful for the intact disc owing to the end effect observed in this study.

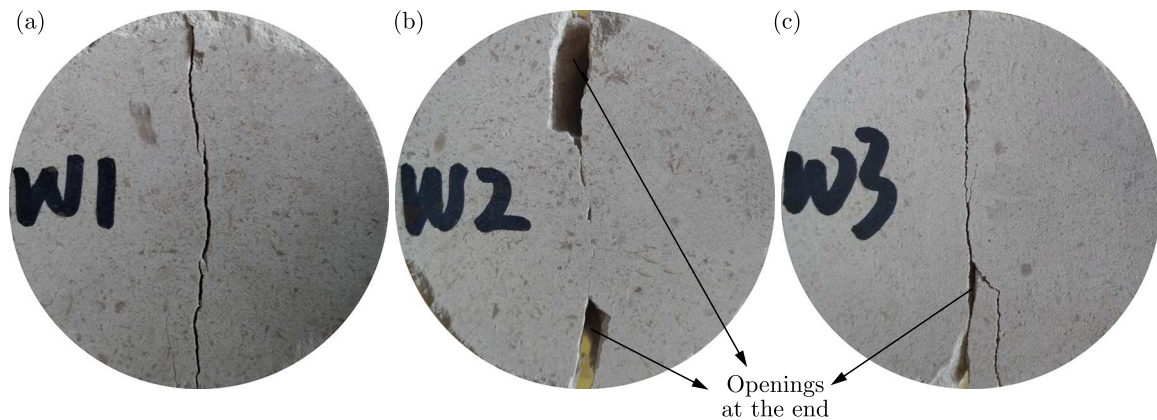


Fig. 3. Failure of intact specimens: (a) specimen W1; (b) specimen W2; (c) specimen W3

### 3.2. Strength of the holed disc

The relationship between the peak load and the ratio of the diameter of the center hole to that of the disc  $d/D$  for C-specimens is presented in Fig. 4a. The results indicate that with the increasing diameter  $d$  of the center hole, the peak load of the discs decreases gradually, especially when the ratio  $d/D$  is less than 0.12. When the ratio  $d/D$  is greater than 0.2, the peak load decreases rapidly. However, for the ratio  $d/D$  in the range of 0.12 to 0.2, the peak load has only a small reduction from 4.32 kN to 4.08 kN (the average values of two of the same specimens, the

same below) with a decrease of approximately 5.55%. With an increase in the diameter ratio  $d/D$  ranging from 0.08 to 0.12 and 0.2 to 0.24, the peak load decreases by 18.48% and 33.09%, respectively.

The relationship of the peak load versus the eccentricity for EH-specimens is presented in Fig. 4b. The curve demonstrates that the peak load of EH-specimens generally increases with the increasing eccentricity when  $2b/D$  is less than 0.4. However, the peak load reaches a plateau after the ratio  $2b/D$  exceeds 0.4. As a result, for the discs with a horizontally eccentric hole, when the eccentricity is larger than 0.4 times the radius (50 mm) of discs, the hole has little or even no effect on the peak load.

With an increased inclination angle  $\alpha$  for the ER-specimen, the peak load exhibits first a slight increase and then gradually decreases, with a maximum of 9.02 kN and a minimum of 4.67 kN observed at  $\alpha = 15^\circ$  and  $90^\circ$  separately, as shown in Fig. 4c. The average peak load of the ER-specimens with an inclination angle of  $15^\circ$  is 9.02 kN, which is close to 9.45 kN of the intact specimens. Thus, the tensile stress around the hole has the maximum value when the hole is located on the vertical diameter of the disc while the hole with an inclination angle less than  $45^\circ$  has little effect on the peak load of the discs.

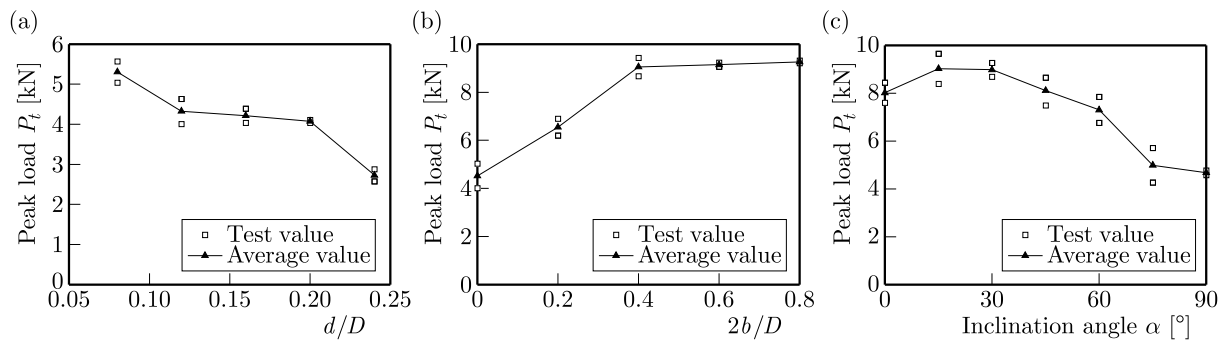


Fig. 4. Peak load of the disc containing a hole versus (a) the ratio of  $d/D$  ( $\alpha = 0^\circ$  and  $b = 0$  mm); (b) the ratio of  $2b/D$  ( $\alpha = 0^\circ$  and  $d = 6$  mm) and (c) the inclination angle  $\alpha$  ( $b = 15$  mm and  $d = 6$  mm)

### 3.3. Failure of the holed disc

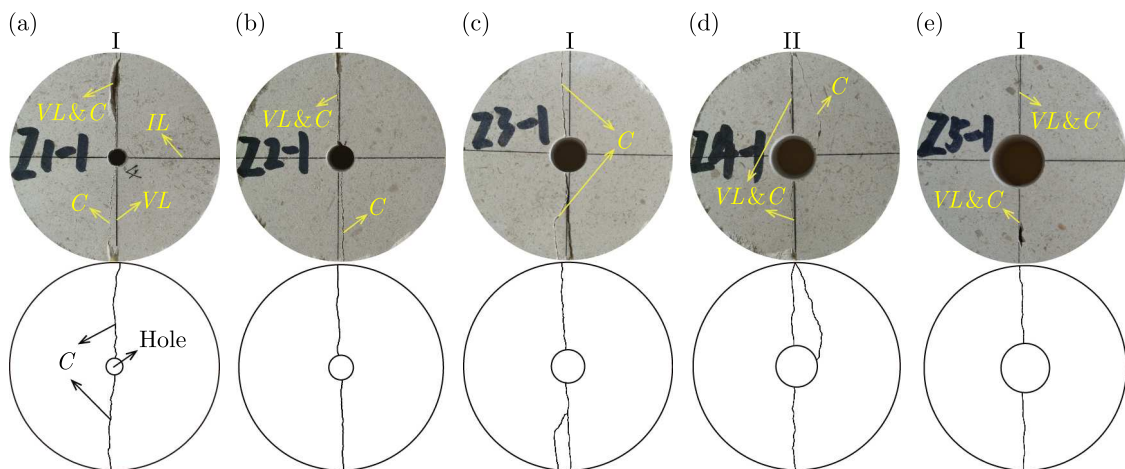


Fig. 5. Failure patterns of C-specimens ( $\alpha = 0^\circ$  and  $b = 0$ ): (a)  $d/D = 0.08$ ; (b)  $d/D = 0.12$ ; (c)  $d/D = 0.16$ ; (d)  $d/D = 0.20$ ; (e)  $d/D = 0.24$ . Note: above is the failure pattern and below is the sketch; VL and IL represent marked/referenced lines; C denotes a crack; I and II denote failure pattern I and failure pattern II, respectively

Figures 5 and 6 show the failure patterns of the holed specimens, which can be classified into five types, illustrated in Table 2.

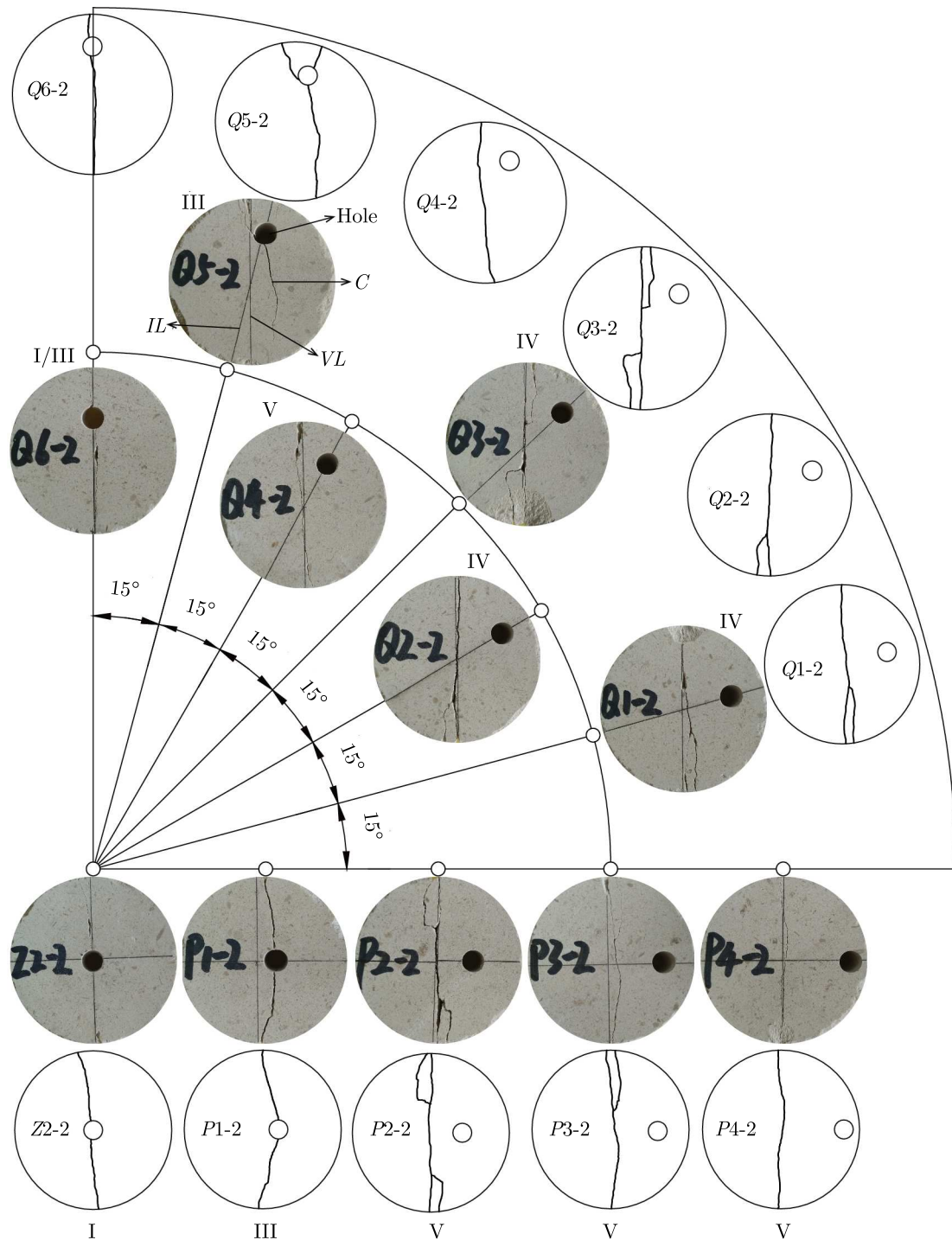
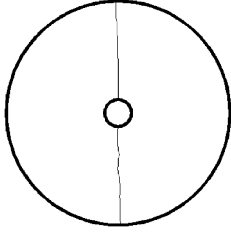
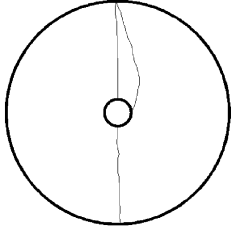
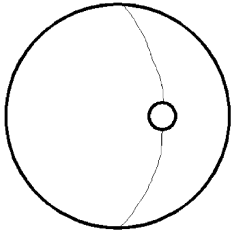
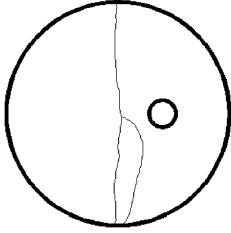
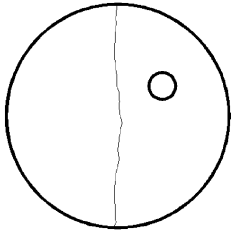


Fig. 6. Failure patterns of EH-specimens ( $\alpha = 0^\circ$  and  $d = 6$  mm) and ER-specimens ( $b = 15$  mm and  $d = 6$  mm). Note: I, III, IV and V represent failure patterns I, III, IV and V, respectively

The characteristics of each failure pattern are described as follows.

**Failure pattern I:** Two cracks propagate in a straight manner in the load direction. The straight cracks connect the points at the top and bottom of the hole with the upper and lower loading points. This failure pattern is found only when the hole is located at the vertical diameter of the discs, e.g., the C-specimens except for the specimen of Z4-1 and the

**Table 2.** Failure patterns of the holed discs

Failure pattern	Specimens	Characteristics
I	 <p>Z1-1, Z1-2 (C-specimen, <math>d = 4</math> mm)  Z2-1, Z2-2 (C-specimen, <math>d = 6</math> mm)  Z3-1, Z3-2 (C-specimen, <math>d = 8</math> mm)  Z5-1, Z5-2 (C-specimen, <math>d = 12</math> mm)  Q6-1, Q6-2 (ER-specimen, <math>\alpha = 90^\circ</math>)</p>	<ul style="list-style-type: none"> <li>• Two straight cracks</li> <li>• Cracking along the load line</li> <li>• Initiated from and propagated through the top and the bottom of the hole</li> </ul>
II	 <p>Z4-1, Z4-2 (C-specimen, <math>d = 10</math> mm)</p>	<ul style="list-style-type: none"> <li>• Two straight cracks and an arc crack</li> <li>• The straight cracks are similar to the two in pattern I</li> <li>• The arc crack passes through a loading point at the left or right side of the hole</li> </ul>
III	 <p>P1-1, P1-2 (EH-specimen, <math>b = 5</math> mm)  Q4-1 (ER-specimen, <math>\alpha = 60^\circ</math>)  Q5-1, Q5-2 (ER-specimen, <math>\alpha = 75^\circ</math>)  Q6-1, Q6-2 (ER-specimen, <math>\alpha = 90^\circ</math>)</p>	<ul style="list-style-type: none"> <li>• An arc ipsilateral crack pair</li> <li>• The endpoints of the arc cracks are the top or bottom of the hole and the position close to/at one of the load points</li> <li>• Two arc cracks have an approximately top-bottom symmetric distribution with the axis of the horizontal diameter</li> </ul>
IV	 <p>P2-1, P2-2 (EH-specimen, <math>b = 10</math> mm)  P3-1, P3-2 (EH-specimen, <math>b = 15</math> mm)  Q1-1, Q1-2 (ER-specimen, <math>\alpha = 15^\circ</math>)  Q2-1, Q2-2 (ER-specimen, <math>\alpha = 30^\circ</math>)  Q3-1, Q3-2 (ER-specimen, <math>\alpha = 45^\circ</math>)</p>	<ul style="list-style-type: none"> <li>• An approximately straight crack and an arc crack</li> <li>• The approximately straight crack propagates in the loading direction</li> <li>• The arc crack passes through the loading point and points to the hole, then turns to the line of loading and coalesces at a point that lies on the straight crack</li> </ul>
V	 <p>P4-1, P4-2 (EH-specimen, <math>b = 20</math> mm)  Q4-2 (ER-specimen, <math>\alpha = 60^\circ</math>)</p>	<ul style="list-style-type: none"> <li>• An approximately straight crack</li> </ul>

ER-specimens with an inclination angle of  $90^\circ$  (namely Q6-1 and Q6-2). Notably, there is no conspicuous opening failure at the specimen boundary adjacent to loading points, which might suggest that the straight cracks initiated at the wall of the hole and propagated towards the loading points along the vertical diameter direction.

**Failure pattern II:** Three cracks including two straight cracks and one arc crack developed. This failure pattern appears only in the C-specimens with a hole diameter of 10 mm, whereas pattern I occurred in all other C-specimens. The two straight cracks are similar to the features of pattern I in formation, and the arc crack connected one of the load points and the left/right side of the hole.

**Failure pattern III:** An arc ipsilateral crack pair developed at the upper and lower halves of the specimen separately. The two arc cracks exhibited an approximately up-down symmetric distribution with the axis of the horizontal diameter. The endpoints of the arc cracks were the top or bottom of the hole boundary and the position close to/at one of the load points. This failure pattern occurred in the EH-specimens of  $2b/D = 0.2$  and the ER-specimens of  $\alpha \geq 60^\circ$ . In addition, one of the ER-specimens with an  $\alpha$  of  $60^\circ$  was also fractured with that pattern, but the failure of the other ER-specimens exhibited failure pattern IV (described in the next section). Because of the special position of the hole in specimens Q6-1 and Q6-2 (ER-specimens with  $\alpha$  of  $90^\circ$ ), their failure patterns are classified into failure pattern III and pattern I.

**Failure pattern IV:** This failure pattern is similar to the failure features of the intact specimens. The main crack (approximately straight) grew in the vertical diameter of the disc, and a secondary arc crack developed at the position adjacent to the loading point. The arc crack intersected with the approximately straight crack, and one of the endpoints of the arc crack was one of the loading points. That failure pattern primarily occurred in the EH-specimens with  $2b/D = 0.4$  and  $0.6$  and the ER-specimens of  $\alpha \leq 45^\circ$ .

**Failure pattern V:** For the EH-specimen with the eccentricity  $b$  of 20 mm (where the ratio of  $2b/D = 0.8$ ), only an approximately straight crack was produced along the vertical diameter direction, which was similar to the intact specimen W1. In addition, the specimen numbered Q4-2 with  $\alpha$  of  $60^\circ$  also broke with that failure pattern.

Based on the above observations, the following can be concluded:

- The failure of all the C-specimens occurred under failure pattern I except for the specimens with a hole diameter of 10 mm, which followed pattern II.
- Three failure patterns appeared in the EH-specimens with different eccentricity  $b$ : when the disc had an eccentricity of 0 (i.e., C-specimen), pattern I occurred. With an increased eccentricity, the failure pattern developed into pattern III ( $b = 5$  mm) and pattern IV ( $b = 10$  mm and  $15$  mm). When the eccentricity  $b$  was 20 mm, failure pattern V occurred.
- The ER-specimens had four failure patterns changing from pattern IV ( $\alpha = 10^\circ, 30^\circ$  and  $45^\circ$ ) to pattern V ( $\alpha = 60^\circ$ ), pattern III ( $\alpha = 60^\circ, 75^\circ$  and  $90^\circ$ ) and pattern I ( $\alpha = 90^\circ$ ) with the increasing inclination angle  $\alpha$ .

#### 4. Numerical modeling to determine the location of crack initiation

According to the test results, the peak loads and the failure patterns of the holed discs are affected by the parameters of the hole diameter  $d$ , the eccentricity  $b$ , and the inclination angle  $\alpha$ . The characteristics of the crack initiation in Brazilian discs are the basis for studies of fracture mechanical properties. Based on the basic theory of fracture mechanics, the potential location

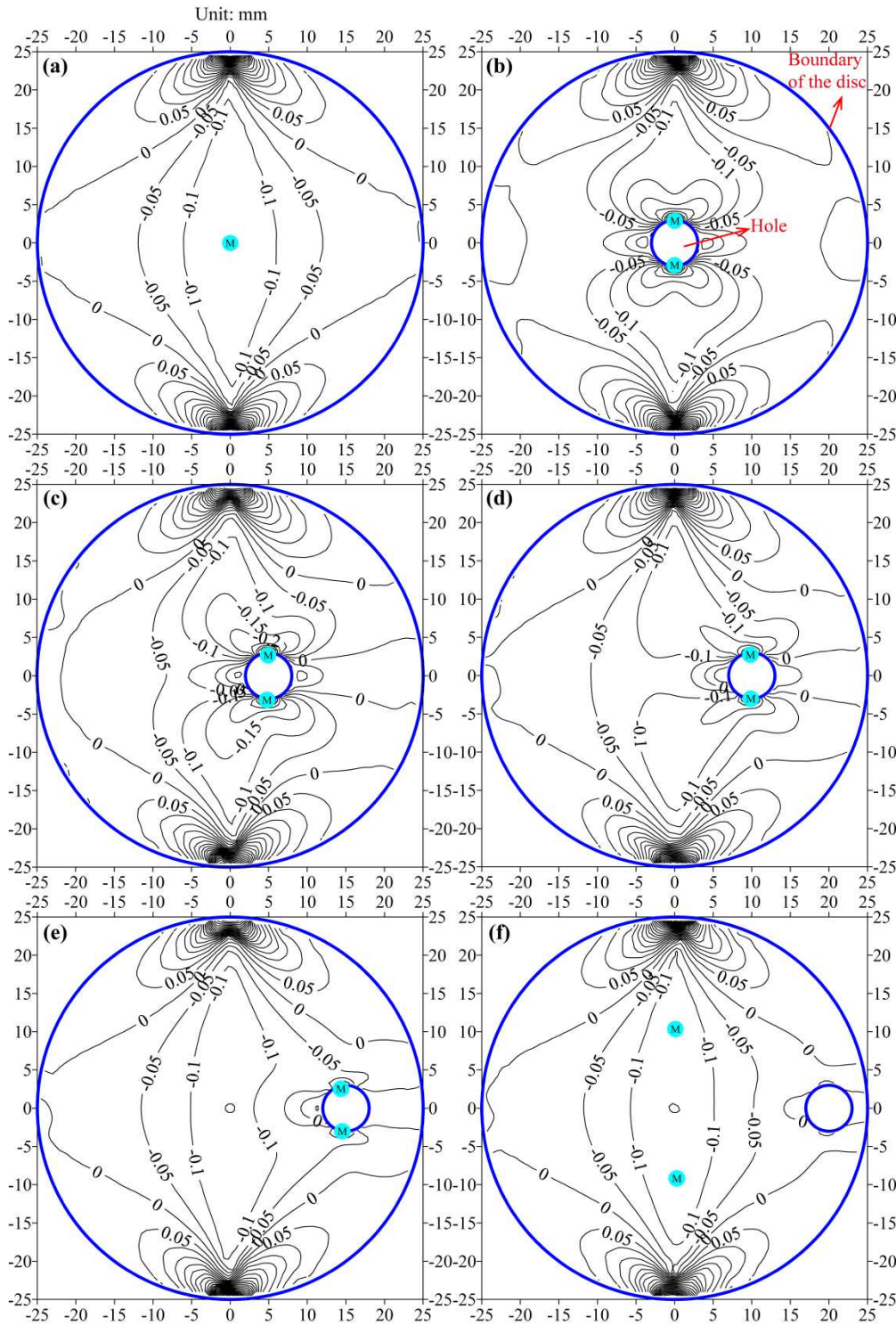


Fig. 7. Contour plots of the horizontal stress (compressive stress is positive, and tensile stress is negative) of the (a) intact disc and EH-specimen with an eccentricity of (b)  $b = 0$ , (c)  $2b/D = 0.2$ , (d)  $2b/D = 0.4$ , (e)  $2b/D = 0.6$ , (f)  $2b/D = 0.8$ . Note: EH-specimens have the same hole diameter of 6 mm;  $\textcircled{M}$  is the position of maximum tensile stress

of crack initiation in a disc specimen is where the tensile stress is maximal. Therefore, the finite element method (FEM) is used to analyze the distribution of the horizontal stress, particularly tensile stress in the holed disc specimens. The geometry of discs built in ANSYS was the same as for the experimental specimens, i.e., the hole diameter  $d$  of the C-specimen ranged from 4

to 12 mm with an interval of 2 mm, the eccentricity  $b$  ranged from 0 to 20 mm with an interval of 5 mm in the EH-specimens (hole diameter  $d = 6$  mm) and the inclination angle  $\alpha$  ranged from  $0^\circ$  to  $90^\circ$  with an interval of  $15^\circ$  for the ER-specimens. The 2D linear elastic constitutive model was adopted in ANSYS to reveal the distribution of stress in the holed discs. In accordance with the Brazilian split test method, a pair of balanced point loads of 10 kN was applied in the vertical diameter direction, which was approximately the peak load of the tested intact specimens. The linear-elastic model constructed for simulation had Poisson's ratio and Young's modulus of 0.25 and 5.12 GPa, respectively. Poisson's ratio and Young's modulus used here were the same as those of the rock samples measured by uniaxial compression test.

The contour plots of horizontal stress of the numerical simulations are illustrated in Figs. 7 and 8, where compressive stress is positive and tensile stress is negative, and the position of the maximum tensile stress is marked by a circled letter M. The variations in the maximum tensile stress with the diameter  $d$  of the center hole, the eccentricity  $b$  and the inclination angle  $\alpha$  are presented in Fig. 9. Within the intact disc, the horizontal stress exhibits a symmetrical distribution with the vertical and horizontal diameter line of the disc as the axis of symmetry (Fig. 7a). At the positions adjacent to the load points, the horizontal stress shows compression. The tensile stress appears in other areas, especially at the center of the disc where a maximum value of 0.13 MPa is observed.

Within the C-specimen, except for the locations near the load points, most of other regions exhibit tensile stress, as shown in Fig. 7b. The contour of tensile stress exhibits an "8" shape, and the center of the "8" is located at the hole around which the maximum tensile stress is attained due to concentration of stress. The horizontal stress distributions are similar and only differ in values within the C-specimens. Thus, the horizontal stress of the C-specimen with a diameter of 6 mm is illustrated in Fig. 7b. As shown in Fig. 9a, as the ratio  $d/D$  is increased from 0.08 to 0.24, the maximum tensile stress exhibits a distinct increase from 0.69 to 0.95 MPa, an increase of approximately 37.68%. This explains the decrease in the peak load of the C-specimen with an increased diameter of the central hole (See Fig. 4a).

The horizontal stress and the position of the maximum tensile stress in the EH-specimens change gradually with the eccentricity, as shown in Figs. 7 and 9b, respectively. However, the maximum tensile stress always appears at the boundary of the hole, except for the EH-specimen with the ratio  $2b/D$  of 0.8 ( $b = 20$  mm), for which the maximum is at a point located at the vertical load line and off the center of the disc (Fig. 7f). That explains why the failure pattern of the EH-specimen evolves from a straight crack to an arc crack then back to a straight crack again with an increased eccentricity  $b$ . The maximum tensile stress of the EH-specimen decreases with the eccentricity, and when the ratio  $2b/D$  is 0.8, the maximum is 0.13 MPa, which is equal to that of the intact disc. This finding agrees with the variation in the peak load presented in Fig. 4b, which exhibits a gradual increase tending toward the peak load of the intact disc. For the ER-specimens, the maximum tensile stresses are all observed at the boundary of the hole (Fig. 8). Only a negligible decrease of 0.41% is found when the inclination angle  $\alpha$  increases from  $0^\circ$  to  $15^\circ$ , which explains why the peak load of the ER-specimens exhibits only a slight increase between the angle intervals presented in Fig. 4c.

An interesting characteristic of the horizontal stress in the holed discs from the FEM simulation is that almost all the locations of the maximum tensile stress are at the boundary of the hole except the EH-specimen with an eccentricity of 20 mm. In addition, the angle  $\beta$  defined in Fig. 10a is the deflection angle of the segment between the center of the hole and the point of crack initiation (namely maximum tensile stress, when there are two maximums the point refers to above that point) off the vertical radius line of the disc. The changes of the  $\beta$  with the eccentricity  $b$  and the inclination angle  $\alpha$  are shown in Figs. 10b and 10c. When the ratio  $2b/D$  is 0 or 0.2, the  $\beta$  is  $0^\circ$ , which means that the position of the maximum tensile stress is located at the boundary point of the vertical diameter of the hole. As the ratio  $2b/D$  is increased from 0.4

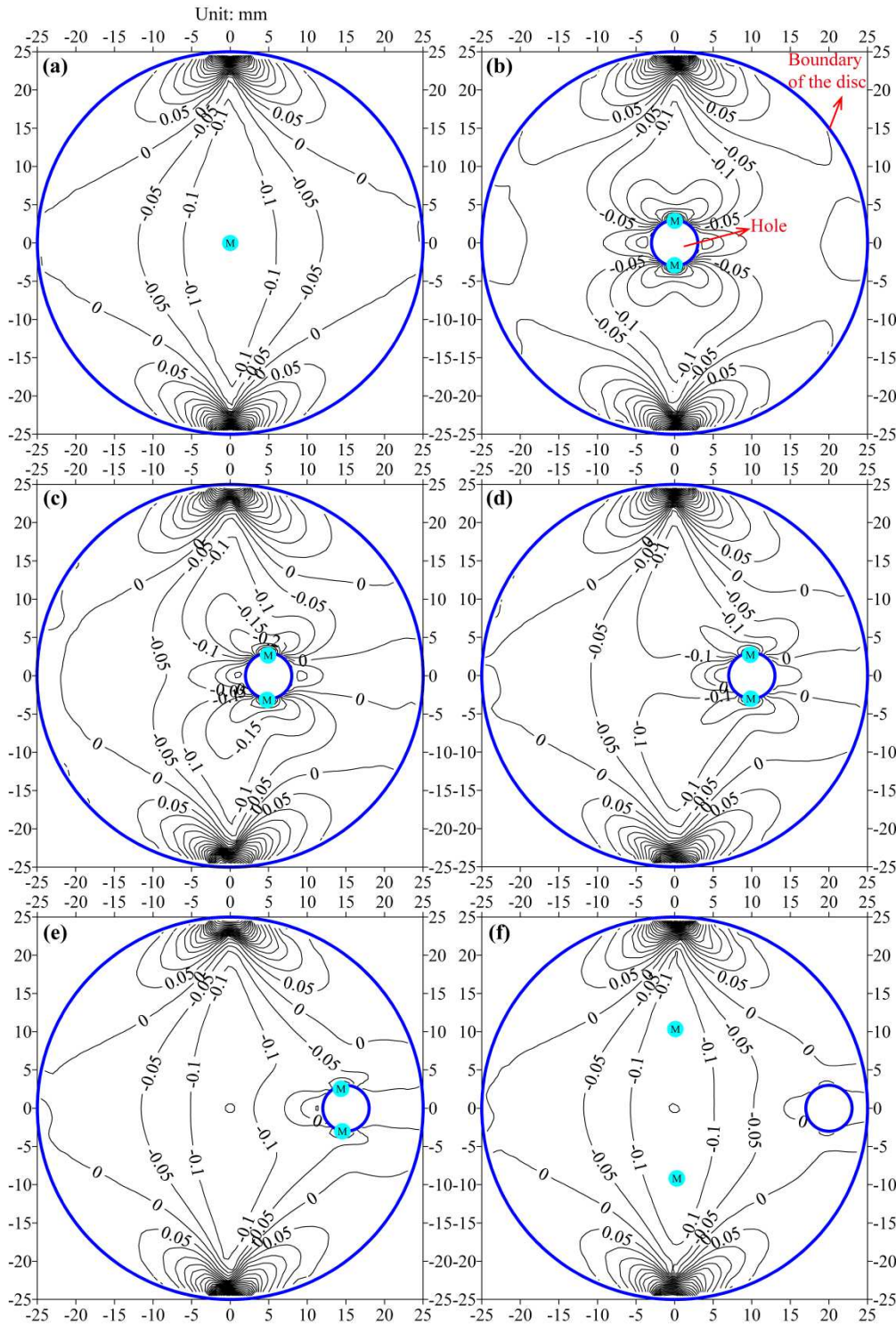


Fig. 8. Contour plots of the horizontal stress of the ER-specimens with inclination angles of (a)  $\alpha = 15^\circ$ , (b)  $\alpha = 30^\circ$ , (c)  $\alpha = 45^\circ$ , (d)  $\alpha = 60^\circ$ , (e)  $\alpha = 75^\circ$ , and (f)  $\alpha = 90^\circ$ ;  $\textcircled{M}$  is the position of maximum tensile stress

to 0.6, the deflection angle  $\beta$  increases from  $6.51^\circ$  to  $13.05^\circ$ . When the ratio is 0.8, the position of the maximum tensile stress lies on the vertical load line, and the angle  $\beta$  increases to  $63.89^\circ$ .

For the ER-specimens (Fig. 10c), the angle  $\beta$  increases after first decreasing and then decreases again with an increased inclination angle  $\alpha$ . The maximum  $\beta$  is approximately  $25^\circ$ - $26^\circ$  in the cases of  $\alpha$  ranging from  $45^\circ$  to  $60^\circ$ . The angle  $\beta$  achieves a minimum of  $0^\circ$  when  $\alpha = 90^\circ$ .

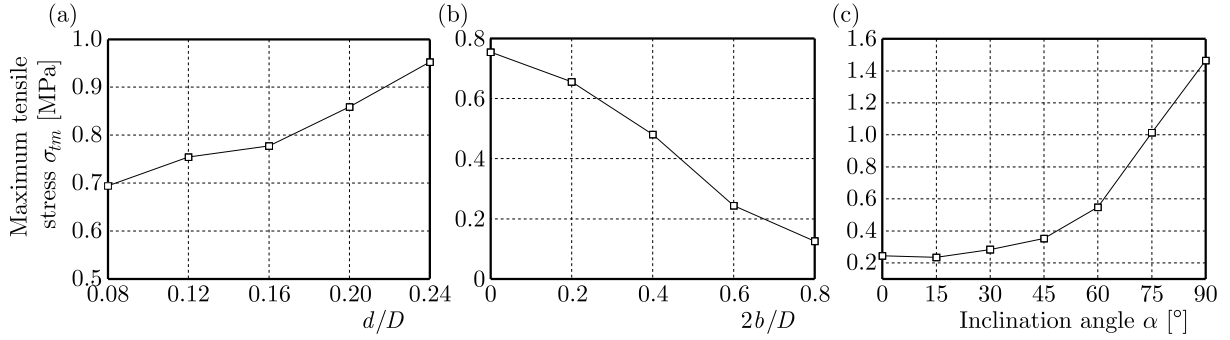


Fig. 9. Variation in the maximum tensile stress (absolute value) of (a) C-specimen, (b) EH-specimen, (c) ER-specimen

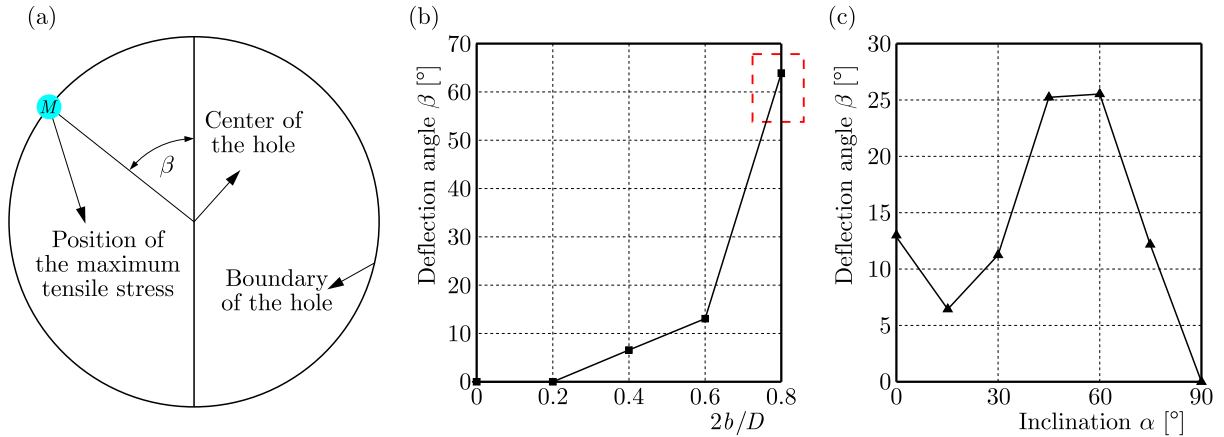


Fig. 10. (a) Sketch of the position of the maximum tensile stress at the boundary of the hole.

Note:  $\beta$  is the deflection angle of the segment between the center of the hole and the point of the maximum tensile stress off the upper vertical radius. Curves of the deflection angle  $\beta$  versus the ratio of (b)  $2b/D$  and (c) the inclination angle  $\alpha$

## 5. Conclusions

- The three parameters of the holes – diameter  $d$ , eccentricity  $b$  and the inclination angle  $\alpha$  – have significant influences on the peak load and the failure pattern of the holed discs. The peak load decreases with the increasing diameter of the central hole. The peak load of the EH-specimens gradually increases to that of intact specimens with the increasing eccentricity  $b$ . For the ER-specimen, the peak load exhibits first a slight increase and then a distinct decrease with the increasing inclination angle  $\alpha$  (the maximum is observed at  $\alpha = 15^\circ$  and  $30^\circ$ , and the minimum is found at  $\alpha = 90^\circ$ ).
- When the holes are located along the vertical diameter of the discs, i.e., the C-specimens and the ER-specimens with an inclination angle  $\alpha$  of  $90^\circ$ , the failure pattern generally exhibits two straight cracks between the top and bottom sides of the hole and load points. For the EH-specimens, with the increasing eccentricity  $b$ , the failure is characterized by the pattern changing from two straight cracks to an arc crack and then a straight crack again. The failure of the ER-specimens is similar to that of the EH-specimens, but the ends of the discs do not evolve into a straight crack.
- The position and value of the maximum tensile stress changes with the eccentricity  $b$  and the inclination angle  $\alpha$ . All the positions are located on the boundaries of the holes. There is a deflection angle  $\beta$  between the upper vertical radius of the holes and the connecting line of the position of the maximum tensile stress and the center of the holes. The angle  $\beta$  increases as the ratio  $2b/d$  increases. With the increasing inclination angle  $\alpha$ , the angle  $\beta$

first decreases and then decreases again after an obvious increase when the angle  $\alpha$  ranges from  $15^\circ$  to  $60^\circ$ . When the hole lies at the center of the disc, the angle  $\beta$  has a constant value of  $0^\circ$ . Variations in the stress field and the position of the maximum horizontal tensile stress result in different failure patterns.

#### Acknowledgments

This work has been supported by the Fundamental Research Funds for the Central Universities (No. 106112017CDJXSYY002), the Graduate Research and Innovation Foundation of Chongqing, China (No. CYB17043), the National Natural Science Foundation of China (No. 41472245, 41672300), the Scientific Research Foundation of State Key Lab. of Coal Mine Disaster Dynamics and Control (No. 2011DA105287-MS201502).

#### References

1. CAI M., 2013: Fracture initiation and propagation in a Brazilian disc with a plane interface: a numerical study, *Rock Mechanics and Rock Engineering*, **46**, 289-302
2. DAI F., CHEN R., IQBAL M.J., XIA K., 2010: Dynamic cracked chevron notched Brazilian disc method for measuring rock fracture parameters, *International Journal of Rock Mechanics and Mining Sciences*, **47**, 606-613
3. FAIRHURST C., 1964: On the validity of the 'Brazilian' test for brittle materials, *International Journal of Rock Mechanics and Mining Science and Geomechanics Abstracts*, **1**, 535-546
4. FISCHER M.P., ALLEY R.B., ENGELDER T., 1995, Fracture toughness of ice and firn determined from the modified ring test, *Journal of Glaciology*, **41**, 383-394
5. FOWELL R.J., 1995, Suggested method for determining mode I fracture toughness using Cracked Chevron Notched Brazilian Disc (CCNBD) specimens, *International Journal of Rock Mechanics and Mining Sciences and Geomechanics Abstracts*, **32**, 57-64
6. HOBBS D.W., 1964, The tensile strength of rocks, *International Journal of Rock Mechanics and Mining Science and Geomechanics Abstracts*, **1**, 385-396
7. HOBBS D.W., 1965, An assessment of a technique for determining the tensile strength of rock, *British Journal of Applied Physics*, **16**, 259-268
8. HOSSAIN A.B., WEISS J., 2006, The role of specimen geometry and boundary conditions on stress development and cracking in the restrained ring test, *Cement and Concrete Research*, **36**, 189-199
9. HUA W., LI Y., DONG S., LI N., WANG Q., 2015, T-stress for a centrally cracked Brazilian disk under confining pressure, *Engineering Fracture Mechanics*, **149**, 37-44
10. HUANG D., ZHU T.T., 2018, Experimental and numerical study on the strength and hybrid fracture of sandstone under tension-shear stress, *Engineering Fracture Mechanics*, **200**, 387-400
11. HUDSON J.A., 1969, Tensile strength and the ring test, *International Journal of Rock Mechanics and Mining Science and Geomechanics Abstracts*, **6**, 91-97
12. ISRM, 1978, Suggested methods for determining tensile strength of rock materials, *International Journal of Rock Mechanics and Mining Science and Geomechanics Abstracts*, **15**, 99-103
13. KELES C., TUTLUOGLU L., 2011, Investigation of proper specimen geometry for mode I fracture toughness testing with flattened Brazilian disc method, *International Journal of Fracture*, **169**, 61-75
14. LAMBERT D.E., ROSS C.A., 2000, Strain rate effects on dynamic fracture and strength, *International Journal of Impact Engineering*, **24**, 985-998
15. LIN H., XIONG W., XIONG Z., GONG F., 2015, Three-dimensional effects in a flattened Brazilian disk test, *International Journal of Rock Mechanics and Mining Sciences*, **74**, 10-14

16. LIN H., XIONG W., YAN Q., 2016, Modified formula for the tensile strength as obtained by the flattened Brazilian disk test, *Rock Mechanics and Rock Engineering*, **49**, 1-8
17. MELLOR M., HAWKES I., 1971, Measurement of tensile strength by diametral compression of discs and annuli, *Engineering Geology*, **5**, 173-225
18. PERRAS M.A., DIEDERICHS M.S., 2014, A review of the tensile strength of rock, concepts and testing, *Geotechnical and Geological Engineering*, **32**, 525-546
19. RIAZI R., TORABI A.R., AMININEJAD S., SABOUR M.H., 2015, Combined tension-shear fracture analysis of V-notches with end holes, *Acta Mechanica*, **226**, 3717-3736
20. SHANG Y., PARK H.D., YUAN G., SUN Y., GAO Q., 2008, From in situ stress and discontinuities to the strength of granites, comparison and case study, *Geosciences Journal*, **12**, 361-372
21. SONG I., SUH M., WON K.S., HAIMSON B., 2001, A laboratory study of hydraulic fracturing breakdown pressure in tablerock sandstone, *Geosciences Journal*, **5**, 263-271
22. STEEN B.D., VERVOORT A., NAPIER J.L., 2005, Observed and simulated fracture pattern in diametrically loaded discs of rock material, *International Journal of Fracture*, **131**, 35-52
23. SURENDRA K.N., SIMHA K.Y., 2013, Design and analysis of novel compression fracture specimen with constant form factor, Edge Cracked Semicircular Disk, ECSD, *Engineering Fracture Mechanics*, **102**, 235-248
24. TONG J., WONG K.Y., LUPTON C., 2007, Determination of interfacial fracture toughness of bone-cement interface using sandwich Brazilian disks, *Engineering Fracture Mechanics*, **74**, 1904-1916
25. WANG S.Y., SLOAN S.W., TANG C.A., 2014, Three-dimensional numerical investigations of the failure mechanism of a rock disc with a central or eccentric hole, *Rock Mechanics and Rock Engineering*, **47**, 2117-2137
26. ZHANG W., GAO L., JIAO X., YU J., SU X., DU S., 2014, Occurrence assessment of earth fissure based on genetic algorithms and artificial neural networks in Su-Xi-Chang land subsidence area, China, *Geosciences Journal*, **18**, 485-493

*Manuscript received November 4, 2017; accepted for print August 1, 2018*